Computational and experimental analysis of a Glaucoma flat drainage device

R.M.R. Panduro[a], Christian Monterrey[b], J.L. Mantari[c,*], Ruth Canahuire[d], H. Alvarez[e], Mario Miranda[f], Ahmed Elsheikh[g]

[a] *Faculty of Mechanical Engineering, Universidad de Ingeniería y Tecnología, Jr. Medrano Silva 165, Barranco, Lima, Perú*
[b] *Departament of Electrical and Mechatronics Engineering, Universidad de Ingeniería y Tecnología, Jr. Medrano Silva 165, Barranco, Lima, Perú*
[c] *Faculty of Mechanical Engineering, National University of Engineering, Av. Túpac Amaru 210, Rimac, Lima, Perú*
[d] *Departament of Electrical and Mechatronics Engineering, Universidad de Ingeniería y Tecnología, Jr. Medrano Silva 165, Barranco, Lima, Perú*
[e] *Faculty of Mechanical Engineering, Universidad de Ingeniería y Tecnología, Jr. Medrano Silva 165, Barranco, Lima, Perú*
[f] *Faculty of Mechanical Engineering, Universidad de Ingeniería y Tecnología, Jr. Medrano Silva 165, Barranco, Lima, Perú*
[g] *School of Engineering, University of Liverpool, UK*

Abstract

This paper presents a computational and experimental analysis of a glaucoma flat drainage device (FDD). The FDD consists of a metallic microplate placed into the eye sclerocorneal limbus, which creates a virtual path between the anterior chamber and its exterior, allowing the intraocular pressure (IOP) to be kept in a normal range. It also uses the surrounding tissue as a flow regulator in order to provide close values of IOP for a wide range of aqueous humor (AH) flow rates. The Neo Hookean hyperelastic model is used for the solid part, while the Reynolds thin film fluid model is used for the fluid part. On the other hand, a gravitational-driven flow test is implemented in order to validate the simulation process. An in-vitro experiment evaluated the flow characteristics of the device implanted in fourteen extirpated pig eyes, giving as a result the best-fit for the Young modulus of the tissue surrounding the device. Finally, according to the resulting computational model, for a range of 1.4-3.1 μL/min, the device presents a pressure variation range of 6-7.5 mmHg.

Keywords: `Glaucoma`, `Fluid-structure interaction`, `Thin-film fluid`, `Glaucoma drainage device (GDD)`, `Finite element method`

*Corresponding author
Email address: `jmantaril@uni.edu.pe` (J.L. Mantari)

1. Introduction

The Glaucoma disease is affects to many humans around the world, being mostly affected people residing in Asia and Africa (Tham et al. (2014)). This illness is defined as a progressive blindness caused by a lesion of the optic nerve due to mainly an abnormal increment of IOP (Casson et al. (2012)). It can initially be treated by using medications such as betablockers, carbonic anhydrase inhibitors, alpha-2 adrenergic agonists and prostaglandin analogs (Inga Samaniego et al. (2017); Li et al. (2016)). However, there are cases where some patients do not tolerate these medications (Mann (2019)), leading to the implantation of a Glaucoma Drainage device (GDD) as last resort.

There is a wide gamma of these kind of implants, such as the Ahmed Glaucoma Valve (AGV), Krupin implant, Molteno device, Baerveldt device, SolX gold shunt, Ex-Press P-50, iStent, CyPass, Hydrus Stent and Glafkos; being the AGV the most used due to its advantage of present the most favorable risk-efficacy profile (Riva et al. (2017)). However, there are some shortcomings that the AGV needs to improve, such as its elevated interval pressure control and its tendency to present obstruction in the micro-pipe. Therefore, new design proposals were presented, such as the Fermat-type spring-mounted micro check valve design developed by Kara & Kutlar (2010), and the flat drainage device invented by Velasquez & Ortiz (2017).

Most of these devices were evaluated by some in-vitro experimental procedures. The most common tests are named gravity-driven flow (GDF) test and syringe-pump-driven flow (SPDF) test. The second one was firstly used by Prata Jr et al. (1995), who analyzed the pressure-flow characteristics of the AGV, Baervelt device, Krupin disk device, the OptiMed glaucoma device and the Molteno dual-chamber implant, being the last one implanted and tested in live rabbits. Results from this research showed that the AGV and Krupin implants worked as pressure regulator valves without a certain position where they are opened or closed. Porter et al. (1997) utilized the gravity-driven flow and syringe-pump-driven flow tests to analyze the drainage behavior of eighteen valved and not valved drainage devices. It was observed that, for non-valved devices, the only one viable test was the SPDF test due to a very reduced pressure resistance presented in the GDF test. The valved devices could be tested using both methods, being the most informative the SPDF test. In addition, those results showed that the flow resistance for both valved and non-valved devices were constant over the collected data range. Later, Estermann et al. (2013) analyzed the flow characteristics of 3 different Ex-PRESS models (P-50, R-50 and P-200) using the GDF test. The flow resistance values presented close values for different pressure conditions, being this characteristic of non-valved drainage devices.

Some researchers designed new tests sharing similarities with the GDF and SPDF tests. For instance, Pan et al. (2003) tested the AGV using a microfluidic modified SPDF test. In that case, three Anopore filters in series were connected to the setup outlet in order to reproduce the in-vivo tissue capsule porosity which encapsulates the AGV outlet. The experiment also worked as a validation

for a Computational Fluid Dynamics (CFD) simulation executed in ANSYS FLUENT, whose results allowed to learn that the frictional pressure losses are negligible. Likewise, Siewert et al. (2013) developed a microfluidic modified GDF test using two hydrostatic fluid columns at the inlet and outlet of the setup, and a flow sensor before the GDD chamber. Kara et al. (2019) pointed that there are some situations that may affects the mentioned in-vitro tests, such as the pipe system flexibility and unwanted syringe pump vibrations. In consequence, they proposed a new microfluidic experimental test setup to overcome those issues. That test included an air compressor connected to a flow control system which let an AH-like fluid circulate from a reservoir to an isolated box in which a GDD is placed. Test configurations are mainly dependent on the GDD structure, being able to be tubular, non-tubular, valved or non-valved.

Additionally, computational simulations are necessary in order to analyze the flow behavior through a GDD. It is well known that the GDD material and the tissue around it play an important role in the flow behavior. This happens due to the non-linear behavior of those materials. Hence, when a fluid-structure analysis is performed, the possibility of a non-linearity of the solid part has to be considered, such as the AGV case, where the solid part is the AGV structure which is made of silicon, a non-linear material. The finite element method (FEM) is one of the most used methods to solve the mentioned cases, including linear materials in general; however, there are other methods that are being studied such as the Galerkin's method, the Rayleigh-Ritz's method, etc. (Al-Furjan et al. (2020); Alimirzaei et al. (2019); Chikr et al. (2020); Hussain et al. (2020); Karami et al. (2019); Shariati et al. (2020a,b)).

Most researchers employed the fluid-structure interaction in order to obtain the GDD flow characteristics. For example, Stay et al. (2005) evaluated the AGV via an in-vitro SPDF test and used its results to validate a CFD model. That model consisted on a fluid-structure analysis; where, for the solid part, a Von Kármán model was considered; and, for the fluid part, a Reynolds model was considered. In addition, the mentioned new GDD model presented by Kara & Kutlar (2010) was also simulated using a software named ANSYS FLUENT. They analyzed all the tubular structure and the compartment where the valve is placed using 2.5D elements. A 3D CFD analysis of the eye was published by Villamarin et al. (2012), where the more important internal parts of the eye were reconstructed using histology images and a case trabeculectomy was also simulated. Furthermore, Mauro et al. analyzed two non-valved GDD devices, the SOLX Gold Micro Shunt and a novel Silicon Shunt device. Those cases were calculated using the Navier-Stokes equations and the Characteristic Based Split scheme Arpino et al. (2011) to analyse the fluid and porous medias.

As it was explained, there are several numbers of experimental tests oriented to evaluate the GDDs flow characteristics. Some results from these tests are employed to compare and improve existent designs or to create new devices. For that reason, the authors believe that the present article would help other researchers to improve new tests configurations and to create new devices based on the GDD analyzed in the present work.

In the present research, experimental and computational analyses of the

FDD are presented. The GDF test is implemented in order to obtain its flow characteristics and compare the results with a reduced fluid-solid coupled FEM model. The experimental procedure considered the device in an extirpated pig eye, with all the assemble submerged under saline solution. On the other hand, the FEM models considered the fluid part to be the AH flowing around the solid device; and the solid part corresponds to be the tissue surrounding the device, which works as a flow regulator of the AH.

This paper is organized as follows. The experimental methodology is explained in Section 2. In Section 3, the numerical model used to represent the physical phenomena in the device is detailed. Then, the results are discussed in Section 4. Finally, the conclusion and representative references are provided.

2. Methodology

2.1. Flat drainage device

The FDD consists of a stainless-steel device inserted into the sclerocorneal limbus. When it is folded on a plane, it has an external size of 4.2mm x 2mm x 0.12mm. This device allows the AH to create a virtual path between the metal sheet and the tissue around it, as it shown in Fig. 1. From this figure, it has to be pointed that the section A works as a tip to help the FDD pierce the tissue; and the section C works as a support for the device and help the AH to be drained through the sclera porosity. The tissue around the FDD section B, shown in the mentioned figure, works as an AH flow regulator, just like the two opposite-facing sheet in the AGV (Stay et al. (2005)). Hence, it is expected the AH flow rate and the equilibrium pressure drop to keep a non-linear relation. The virtual gap between the FDD and its surrounding tissue is created due to a pressure gradient between the eye anterior chamber and the FDD section B end. The AH flow start to increase until the system is in steady state, which happens when the flow at the FDD section B entrance and exit have the same value.

2.2. Gravitational-driven flow test

The GDF test implemented in this paper, consists on the FDD being subjected to a column of fluid while it is implanted into an extirpated pig eye (Fig. 2). The fluid used is an isotonic serum, which is mainly pure water with 0.9% of NaCl, due to its similarities with the AH. The fluid pressure forces the tissue around the device to create a virtual path where the liquid can be drained. The standpipe has a diameter of 4 mm and provides an initial fluid pressure of 40 mmHg.

While the pressure starts to decrease, its value is registered for different values of time until a pressure of 20 mmHg. The data acquisition is done by visual inspection. The justification for this procedure is because of a very prolonged time, more than 1 hour, for the fluid column to be reduced to the mentioned desired pressure value, which reduces drastically the measurement error.

It should be emphasized that the couple eye-FDD (Fig. 3) is kept submerged into isotonic serum during the test to avoid the mechanical properties degradation of the tissue.

During the experiments, it was noticed that the fluid was draining through the device and the pig eye sclera porosity. Hence, the test is performed following two stages. The first one is conducted by subjecting only the eye to a column of fluid, and the second one by using the same eye with the FDD implanted. The fluid column refill between these two tests is executed with help of a discharge valve showed in Fig. 2; which is mainly a three-way valve that connects the standpipe with the couple eye-FDD when a test is performed, and with the exterior when a fluid column refill is needed for the second stage of the test. By considering the pressure variation results of the two tests, the pressure variation P_D originated by the drainage device is obtained with the following mathematical procedure:

$$Q_{D+S} = A\frac{dh_{D+S}}{dt} \tag{1a}$$

$$Q_D + Q_S = A\frac{dh_{D+S}}{dt} \tag{1b}$$

$$A\frac{dh_D}{dt} + A\frac{dh_S}{dt} = A\frac{dh_{D+S}}{dt} \tag{1c}$$

$$dh_D + dh_S = dh_{D+S} \tag{1d}$$

$$\rho g dh_D + \rho g dh_S = \rho g dh_{D+S} \tag{1e}$$

$$dP_D + dP_S = dP_{D+S} \tag{1f}$$

$$\int_{P_0}^{P_D} dP_D + \int_{P_0}^{P_S} dP_S = \int_{P_0}^{P_{D+S}} dP_{D+S} \tag{1g}$$

$$P_D - P_0 + P_S - P_0 = P_{D+S} - P_0 \tag{1h}$$

$$P_D = P_0 - (P_S - P_{D+S}) \tag{1i}$$

where "D" stands for device, "S" stands for sclera, Q represents the flow, A is the transversal area of the pipe, h is the height of the column of fluid, ρ is the fluid density and g is the acceleration due to gravity. P_0 is the initial pressure imposed by the column of fluid. P_{D+S} and P_S are the pressures registered in the two tests performed to the pig eye alone and the same pig eye with the device implanted respectively. Results of P_D as a function of time are obtained for a total of fourteen pig eyes (Fig. 4).

In order to obtain the pressure variation as a function of flow, the following mathematical procedure is utilized:

$$dP = \rho g dh \tag{2a}$$

$$\frac{dP}{dt} = \rho g \frac{dh}{dt} \tag{2b}$$

$$\frac{dP}{dt} = \rho g \frac{Q}{A} \tag{2c}$$

An exponential equation of P in function of time t is considered:

$$P = \alpha e^{\beta t} + \gamma \tag{3}$$

By using this expression, the following equation is obtained:

$$\alpha\beta e^{\beta t} = \rho g \frac{Q}{A} \tag{4a}$$

$$\beta(P - \gamma) = \rho g \frac{dQ}{dA} \tag{4b}$$

$$P = \rho g \frac{Q}{A\beta} + \gamma \tag{4c}$$

To obtain the values of α, β and γ, the main experimental curve shown in Fig. 4 is fitted with an exponential equation as it is shown in Fig. 5. The resulting relation between P and Q is shown in Fig. 6.

3. Numerical model

Due to the drainage effect occurring mainly in the FDD Section B (Fig. 1), only the flow behavior around that place is analyzed. The FDD dimensions are directly measured from a model donated by Velasquez & Ortiz (2017). As the tissue surrounding the device works as a flow regulator, a fluid-structure interaction analysis is performed. The interactions are executed between the tissue as the solid part, and the AH as the fluid part. The simulation is carried out in the commercial software Comsol Multiphysics 5.4 (COMSOL Inc. (2020)). The AH which flows through the device presents a very reduced thickness in contrary to its side dimensions. Therefore, the use of a 2D reduced model of the Navier-Stokes equation (Bird et al. (2007)) would be more suitable. For instance, the Reynolds equation (Eq. 5), which is mostly used for tribological studies, can be implemented for this study.

$$\nabla . \left(-\frac{w^3}{2\mu^*} \nabla p \right) = 0 \tag{5}$$

where μ^* is the fluid viscosity and p is the value of load pressure. The fluid is considered to have a viscosity of $\mu^* = 1.1cP$ (AH at 25°C) and a density of $\rho = 1000kg/m^3$.

On the other hand, a Neo-Hookean hyperelastic model is utilized to analyze the section of the tissue surrounding the device. The strain energy function selected for this model is as follows:

$$W\left(I_1, J\right) = \frac{\mu}{2}\left(I_1 - 3\right) - \mu ln\left(J\right) + \frac{\lambda}{2}\left(ln\left(J\right)\right)^2 \tag{6}$$

where μ and λ are the Lamé parameters, I_1 is the first invariant and J is the volume ratio. The Lamé parameters are calculated from a specific value of Young modulus E and a Poisson ratio ν, through the following equations:

$$\lambda = \frac{E\nu}{\left(1 + \nu\right)\left(1 - 2\nu\right)} \tag{7}$$

$$\mu = \frac{E}{2\,(1+\nu)} \tag{8}$$

As the tissue behaves like a nearly incompressible material, a Poisson ratio of $\nu = 0.45$ is assumed (Choi & Zheng (2005)). The Young modulus E is calculated by an inverse analysis of the resulting pressures and flows obtained from the GDF test (Fig. 6). This analysis consisted of selecting the pressure of each point of the mentioned plot as an input value for the fluid part, and then performing several runs for a set of E values. The outlet pressure is assumed to be the atmospheric manometric pressure. The modulus value in function of the flow is plotted for each of the mentioned selected points (Fig. 7). Each case in that figure has a different pressure value from the following set of values: 40.0021 mmHg, 35.4284 mmHg, 31.0610 mmHg, 26.9381 mmHg, 25.3708 mmHg, 23.1058 mmHg. After fitting each curve with a 4 order polynomial equation, E is obtained for the corresponding flow value of the previously selected point. Finally, the main value of the resulting modulus group is obtained and used to calculate the Lamé parameters.

The Young modulus obtained from the inverse analysis is $E = 0.0344$ MPa. Therefore, the Lamé Parameters are $\lambda = 0.107$ MPa and $\mu = 0.012$ MPa.

4. Discussions

The experimental and computational analyses of the FDD is performed. For the experimental process, the GDF test is implemented by using extirpated pig eyes with the FDD being implanted. All eye-device couples are pressurized with isotonic serum due to its similarities with the AH. It is ensured that the couple is kept hydrated during the test by filling its support with isotonic serum to avoid a degradation of the eye tissue mechanical properties.

Taking all of these considerations into account, the pressure as a function of time is obtained and shown in Fig. 4. It can be noticed that there are some uncertainties in the results, which are showed as error bars. As the test process is very slow, the acquisition data error are put down at a minimum; however, the error bars are increasing as time goes by. The error increasing is mainly due to variation in the tissue microstructure of the set of pig eyes. As a consequence, it is perceived that at low pressures, the gap between the FDD and the tissue around it is not fully expanded; hence, the gap shape becomes very dependent on the tissue collagen fibers orientation.

Then, it is followed the mathematical process explained in the methodology, in order to obtain the pressure in function of the AH flow rate (Fig. 6). It can be noticed that the pressure and flow present a linear relation. This behavior seems to contradict the variable characteristic variable of the hydraulic resistance of the tissue surrounding the device. However, as these values are obtained from a considerable elevated range of pressures (20-40 mmHg), it is reasonable to obtain a pressure-flow linear relation and consequently a constant hydraulic resistance, due to the fact that the majority of the sclera collagen fibers stopped being wavy to be stretched at those pressure values. Also, it should be noted that

some components of the experimental setup such as the standpipe, the needle and the support provide a pressure drop due to its constant hydraulic resistance. However, considering the mathematical procedure shown in the methodology section, these drops can be included in the expression that represent the pressure variation due to the sclera porosity, which can be cancelled ones the pressure variation due to only the drainage device is obtained.

On the other hand, a non-linear FEM model is implemented in order to obtain the characteristic curve of the drainage device. It is considered a reduced model of the "section B" shown in Fig. 1 which is where the fluid is drained. The reduced model considered the tissue around the device as a Neo-Hookean hyperelastic material. Also, a Poisson coefficient value of 0.45 is considered due to the nearly incompressible behavior of the tissue. The AH is assumed to have a tribological behavior due to a thin film flow created through the tissue and the drainage device. The Reynold equation is implemented as a mathematical expression to represent this behavior. It is considered the fluid to have a viscosity of $\mu^* = 1.1cP$ (AH at 25°C) and a density of $\rho = 1000kg/m^3$. The Lamé parameters which correspond to the sclera section included in the reduced model are obtained from an inverse analysis detailed in the numerical model section.

The simulations are performed using the mesh shown in Fig. 8. The solid part mesh is composed of 13890 hexahedral elements; while the fluid part, whose mesh is taken from the solid part internal surface, is composed of 1200 rectangle elements.

Considering an inlet pressure of 6.5 mmHg and the manometric atmospheric pressure at the outlet, the tissue surrounding the device creates a virtual path of 9.55 μm at each side (Fig. 9). Also, in this case, an AH flow of 1.8663 $\mu L/min$ is obtained. As it is reported by other researchers, the AH production flow presents a value of 2.4 ± 0.6 $\mu L/min$, being greater at the morning and lower at night (Goel et al. (2010)). Hence, the obtained flow value is within the range of a normal eye drainage.

Then, the predicted curve of the pressure variation in function of the fluid flow rate is built. This plot, in conjunction with its experimental counterpart, is shown in Fig. 10. As it can be noticed, the predicted pressure-flow relation keeps a non-linear behavior, being very notorious at low pressures and nearly linear at high values. This nearly linearity at that zone is in accordance with the linear behavior obtained from the experimental process; and, as it was previously explained, this phenomenon is a consequence of multiple tissue collagen fiber stretching at those pressure values. Further, a zoomed area of the low pressure zone from the previously mentioned plot is shown in Fig. 11. For a range of 1.4-3.1 μL/min, the FDD presents a pressure variation range of 6-7.5 mmHg approximately. According to Villamarin et al. (2012), the static pressure imposed at the collecting channels, which is where the AH is conducted after it is drained from the eye anterior chamber, is estimated to be 7 mmHg. Hence, after considering the pressure at the FDD end, the IOP can be obtained by summing the collecting channels pressure to the pressure variation values obtained from the experimental procedure and the simulation. Therefore, the corresponding

IOP of the mentioned pressure variation range of 6-7.5 is 13-14.5 mmHg, which is in agreement with a safety eye IOP condition. Also, in the same figure, the AGV curve, taken from the experimental results of Stay et al. (2005), is superposed. It can be noticed that in the required range of pressure mentioned before, both GDD present nearly the same values; which demonstrate that the FDD can mitigate the glaucoma with the same efficacy of the AGV; however, as the FDD is a non-tubular, it has the advantage of not presenting obstruction.

5. Conclusion

The FDD fluid-structure interaction simulation and its experimental validation using the GDF test was explained. The methodology used in this article allowed to obtain the flow characteristics of the FDD by using a GDF of two stages. This method has the advantage of being very simple, not too much expensive and have low uncertainty in measurements due its large duration; however, it has the main disadvantage of being dependent of the availability of extirpated pig eyes and its results present good accuracy only at high pressures.

According to the results, it is evidenced that the non-linear relation between the FDD and the AH fluid is mainly due to a variable hydraulic resistance imposed by the tissue around the device. However, as the tissue is mainly composed of collagen fibers, they trend to be stretched at high pressures leading to a constant hydraulic resistance at these conditions as it was shown in the experimental and computational results. The FDD is capable of maintain the eye at safety levels of IOP. Also, with help of this study, it was demonstrated that the FDD is as efficient as the AGV, which is the most used GDD. Nevertheless, an in-vivo test would be very useful for a better modelling of the phenomena in the analysis such as a post-operative inflammatory stresses imposed by the tissue in contact with the drainage device.

Acknowledgement

The authors would like to thank to FONDECYT-UK J008-2016 for the financial support during the course of this work.

Nomenclature

$$
\begin{aligned}
FDD &= Flat\ drainage\ device \\
IOP &= Internal\ ocular\ pressure \\
AH &= Aqueous\ humor \\
GDD &= Glaucoma\ drainage\ device \\
AGV &= Ahmed\ glaucoma\ valve \\
GDF &= Gravity - driven\ flow \\
SPDF &= Syringe - pump - driven\ flow \\
CFD &= Computational\ fluid\ dynamics \\
FEM &= Finite\ element\ method \\
P &= Pressure\ [MPa] \\
Q &= Fluid\ flow\ [\mu L/min] \\
D &= Reference\ to\ only\ the\ device \\
S &= Reference\ to\ only\ the\ sclera \\
A &= Transversal\ area\ of\ the\ standpipe\ [mm^2] \\
h &= Height\ of\ the\ column\ of\ fluid\ [mm] \\
\rho &= Fluid\ density\ [kg/m^3] \\
g &= Acceleration\ due\ to\ gravity\ [m/s^2] \\
P_0 &= Initial\ pressure\ imposed\ by\ the\ column\ of\ fluid\ [MPa] \\
t &= Time\ [s] \\
w &= Vertical\ displacement\ [\mu m] \\
\mu^* &= Fluid\ Viscosity\ [cP] \\
W &= Strain\ energy\ function\ [J/m^3] \\
I_1 &= First\ invariant \\
\mu, \lambda &= Lamé\ parameters\ [MPa] \\
J &= Volume\ ratio\ or\ Jacobian \\
\nu &= Poisson\ ratio \\
E &= Young\ modulus\ [MPa]
\end{aligned}
$$

References

Al-Furjan, M., Safarpour, H., Habibi, M., Safarpour, M., & Tounsi, A. (2020). A comprehensive computational approach for nonlinear thermal instability of the electrically FG-GPLRC disk based on GDQ method. *Engineering with Computers*, (pp. 1–18).

Alimirzaei, S., Mohammadimehr, M., & Tounsi, A. (2019). Nonlinear analysis of viscoelastic micro-composite beam with geometrical imperfection using FEM: MSGT electro-magneto-elastic bending, buckling and vibration solutions. *Struct Eng Mech*, *71*, 485–502.

Arpino, F., Massarotti, N., & Mauro, A. (2011). Efficient three-dimensional FEM based algorithm for the solution of convection in partly porous domains. *International Journal of Heat and Mass Transfer*, *54*, 4495–4506.

Bird, R. B., Stewart, W. E., & Lightfoot, E. N. (2007). *Transport phenomena*. John Wiley & Sons.

Casson, R. J., Chidlow, G., Wood, J. P., Crowston, J. G., & Goldberg, I. (2012). Definition of glaucoma: clinical and experimental concepts. *Clinical & experimental ophthalmology*, *40*, 341–349.

Chikr, S. C., Kaci, A., Bousahla, A. A., Bourada, F., Tounsi, A., Bedia, E., Mahmoud, S., Benrahou, K. H., & Tounsi, A. (2020). A novel four-unknown integral model for buckling response of FG sandwich plates resting on elastic foundations under various boundary conditions using Galerkin's approach. *Geomechanics and Engineering*, *21*, 471–487.

Choi, A., & Zheng, Y. (2005). Estimation of Young's modulus and Poisson's ratio of soft tissue from indentation using two different-sized indentors: finite element analysis of the finite deformation effect. *Medical and Biological Engineering and Computing*, *43*, 258–264.

COMSOL Inc. (2020). COMSOL. URL: `http://www.comsol.com/products/multiphysics/`.

Estermann, S., Yuttitham, K., Chen, J. A., Lee, O.-T., & Stamper, R. L. (2013). Comparative in vitro flow study of 3 different Ex-PRESS miniature glaucoma device models. *Journal of glaucoma*, *22*, 209–214.

Goel, M., Picciani, R. G., Lee, R. K., & Bhattacharya, S. K. (2010). Aqueous humor dynamics: a review. *The open ophthalmology journal*, *4*, 52.

Hussain, M., Naeem, M. N., Taj, M., & Tounsi, A. (2020). Simulating vibration of single-walled carbon nanotube using Rayleigh-Ritz's method. *Advances in nano research*, *8*, 215–228.

Inga Samaniego, J., Mantari Laureano, J., Chávez Ávila, F., & Charca Mamani, S. (2017). Benefits and risks of glaucoma drainage devices for glaucoma treatment. *Revista Cubana de Oftalmología*, *30*, 1–12.

Kara, E., & Kutlar, A. (2010). CFD analysis of the Ahmed Glaucoma Valve and design of an alternative device. *Computer methods in biomechanics and biomedical engineering*, *13*, 655–662.

Kara, E., Kutlar, A. İ., & Güngör, K. (2019). Construction of a novel microfluidic experimental setup for testing recent glaucoma drainage devices. *Current Directions in Biomedical Engineering*, *5*, 219–222.

Karami, B., Janghorban, M., & Tounsi, A. (2019). Galerkin's approach for buckling analysis of functionally graded anisotropic nanoplates/different boundary conditions. *Engineering with Computers*, *35*, 1297–1316.

Li, T., Lindsley, K., Rouse, B., Hong, H., Shi, Q., Friedman, D. S., Wormald, R., & Dickersin, K. (2016). Comparative effectiveness of first-line medications for primary open-angle glaucoma: a systematic review and network meta-analysis. *Ophthalmology*, *123*, 129–140.

Mann, E. (2019). Treatment of open-angle glaucoma. *Suicide*, *14*, 20.

Mauro, A., Massarotti, N., Romano, M., Romano, V., & Nithiarasu, P. (). Numerical simulation of suprachoroidal shunts for treatment of glaucoma, .

Pan, T., Li, Z., Brown, J. D., & Ziaie, B. (2003). Microfluidic characterization of a valved glaucoma drainage device with implications for enhanced therapeutic efficacy. In *Proceedings of the 25th Annual International Conference of the IEEE Engineering in Medicine and Biology Society (IEEE Cat. No. 03CH37439)* (pp. 3317–3320). IEEE volume 4.

Porter, J. M., Krawczyk, C. H., & Carey, R. F. (1997). In vitro flow testing of glaucoma drainage devices. *Ophthalmology*, *104*, 1701–1707.

Prata Jr, J. A., Mérmoud, A., LaBree, L., & Minckler, D. S. (1995). In vitro and in vivo flow characteristics of glaucoma drainage implants. *Ophthalmology*, *102*, 894–904.

Riva, I., Roberti, G., Katsanos, A., Oddone, F., & Quaranta, L. (2017). A review of the Ahmed glaucoma valve implant and comparison with other surgical operations. *Advances in therapy*, *34*, 834–847.

Shariati, A., Ghabussi, A., Habibi, M., Safarpour, H., Safarpour, M., Tounsi, A., & Safa, M. (2020a). Extremely large oscillation and nonlinear frequency of a multi-scale hybrid disk resting on nonlinear elastic foundation. *Thin-Walled Structures*, *154*, 106840.

Shariati, A., Habibi, M., Tounsi, A., Safarpour, H., & Safa, M. (2020b). Application of exact continuum size-dependent theory for stability and frequency analysis of a curved cantilevered microtubule by considering viscoelastic properties. *ENGINEERING WITH COMPUTERS*, .

Siewert, S., Becker, C., Schmidt, W., Specht, O., Hinze, U., Chichkov, B., Guthoff, R., & Schmitz, K. (2013). Development of a Test Facility for Microfluidic Characterization of Glaucoma Drainage Devices. *Biomedical Engineering/Biomedizinische Technik*, *58*.

Stay, M. S., Pan, T., Brown, J. D., Ziaie, B., & Barocas, V. H. (2005). Thin-Film Coupled Fluid-Solid Analysis of Flow Through the Ahmed™ Glaucoma Drainage Device. *Journal of biomechanical engineering*, *127*, 776–781.

Tham, Y.-C., Li, X., Wong, T. Y., Quigley, H. A., Aung, T., & Cheng, C.-Y. (2014). Global prevalence of glaucoma and projections of glaucoma burden through 2040: a systematic review and meta-analysis. *Ophthalmology*, *121*, 2081–2090.

Velasquez, M. E. M., & Ortiz, G. E. B. (2017). One piece flat device of for the drainage of aqueous humor from the eye. US Patent App. 15/378,946.

Villamarin, A., Roy, S., Hasballa, R., Vardoulis, O., Reymond, P., & Stergiopulos, N. (2012). 3D simulation of the aqueous flow in the human eye. *Medical engineering & physics*, *34*, 1462–1470.

List of Figures

1 Isometric view of the FDD on the left, FDD placement on the right (Velasquez & Ortiz (2017)) and the donated FDD used in this research on the bottom. 15
2 Gravitational-driven flow test setup. 15
3 Couple eye-FDD. 16
4 Gravitational-driven flow test experimental results. 16
5 Fitted curve of the gravitational flow test results. 17
6 Pressure variation in function of the flow rate obtained from the test results. 17
7 Young modulus in function of flow rate. 18
8 FDD reduced model dimensions on the top and the mesh on the bottom. 19
9 a) Tissue displacements results for the FDD reduced model at a $\Delta P = 6.5mmHg$. b) AH pressure distribution for the FDD reduced model at a $\Delta P = 6.5mmHg$. c) AH velocity distribution for the FDD reduced model at a $\Delta P = 6.5mmHg$ 20
10 Pressure variation in function of the flow rate obtained from the test results and the computational simulation. 21
11 Pressure variation in function of the flow rate obtained from the computational simulation for a range of 0-10 mmHg. 21

Figures

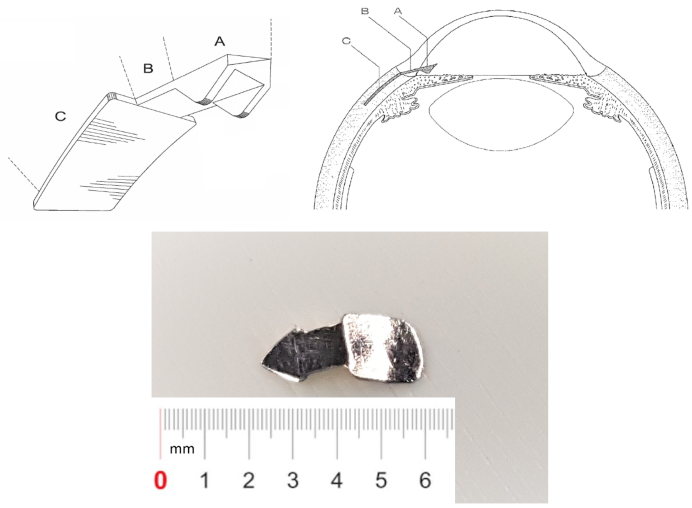

Figure 1: Isometric view of the FDD on the left, FDD placement on the right (Velasquez & Ortiz (2017)) and the donated FDD used in this research on the bottom.

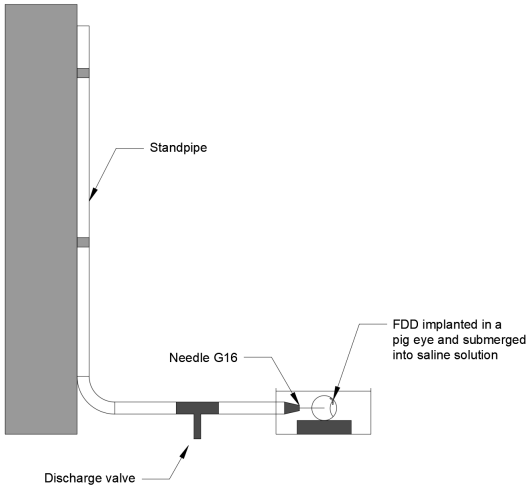

Figure 2: Gravitational-driven flow test setup.

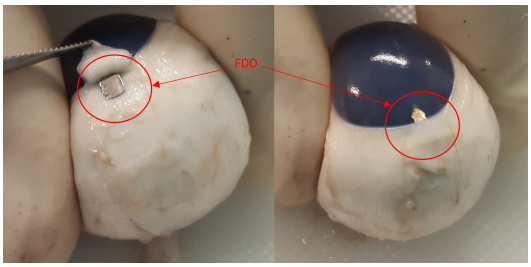

Figure 3: Couple eye-FDD.

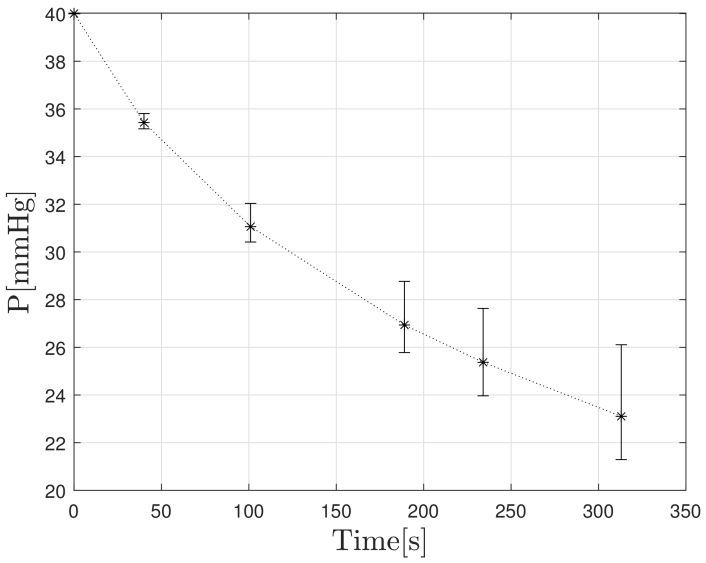

Figure 4: Gravitational-driven flow test experimental results.

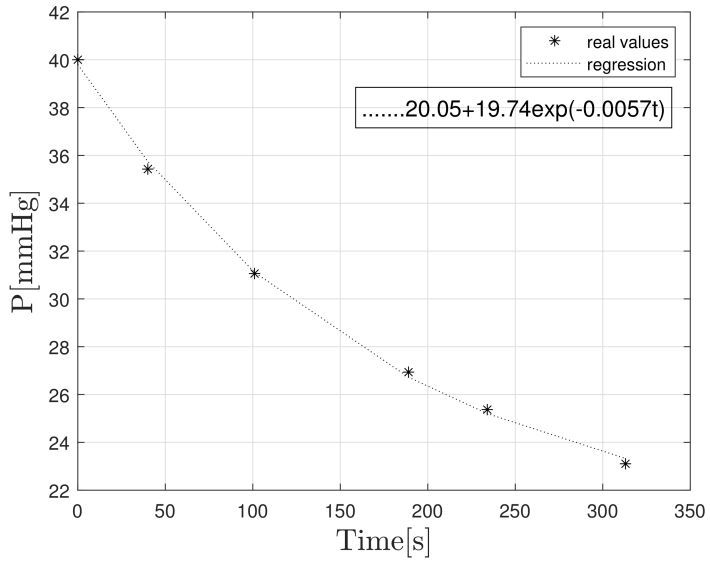

Figure 5: Fitted curve of the gravitational flow test results.

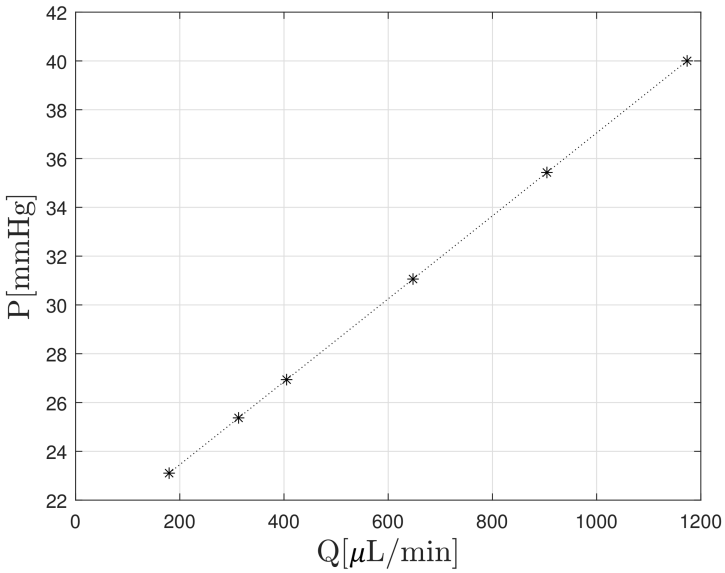

Figure 6: Pressure variation in function of the flow rate obtained from the test results.

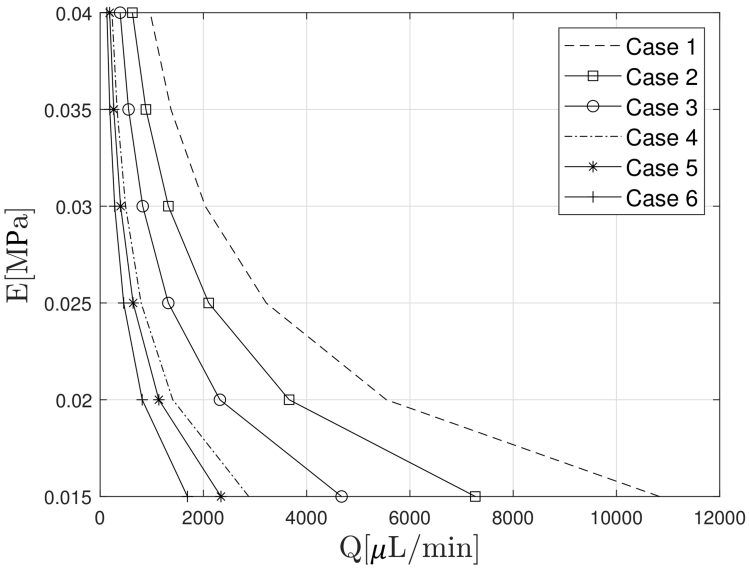

Figure 7: Young modulus in function of flow rate.

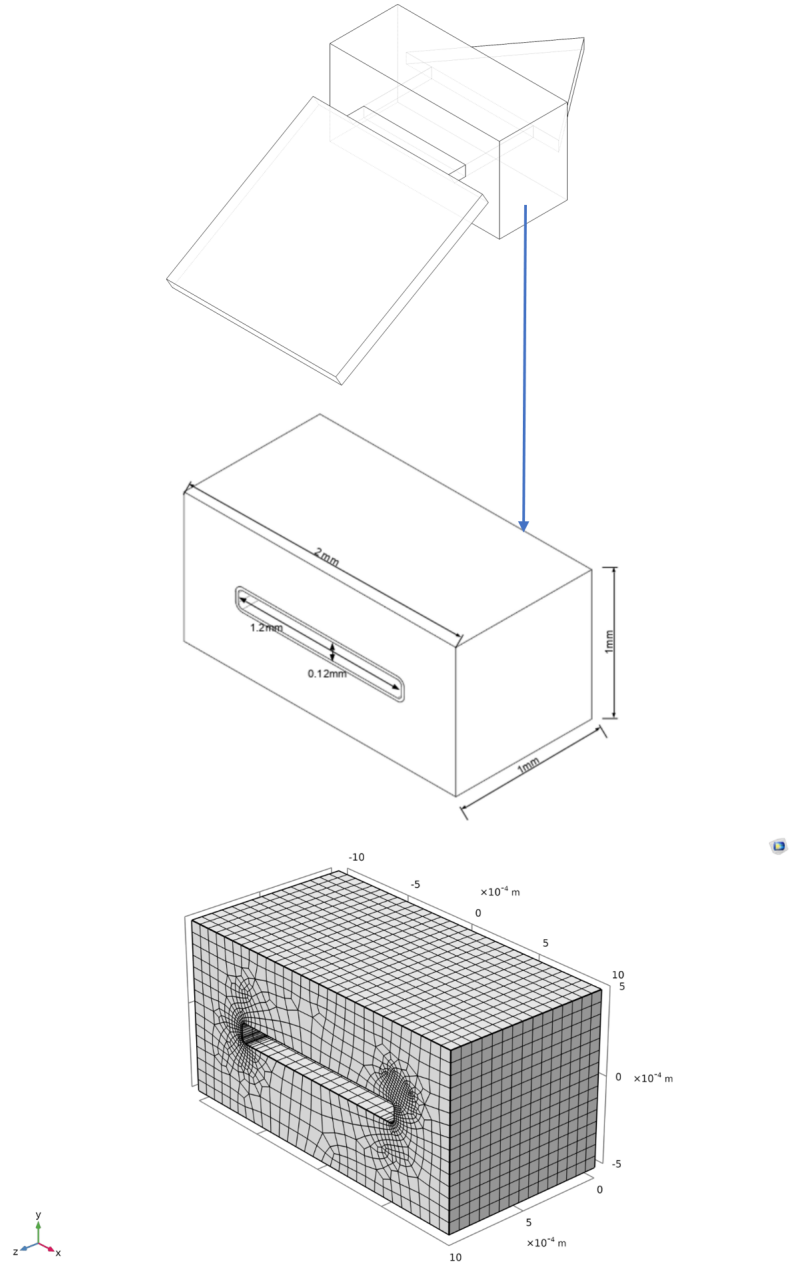

Figure 8: FDD reduced model dimensions on the top and the mesh on the bottom.

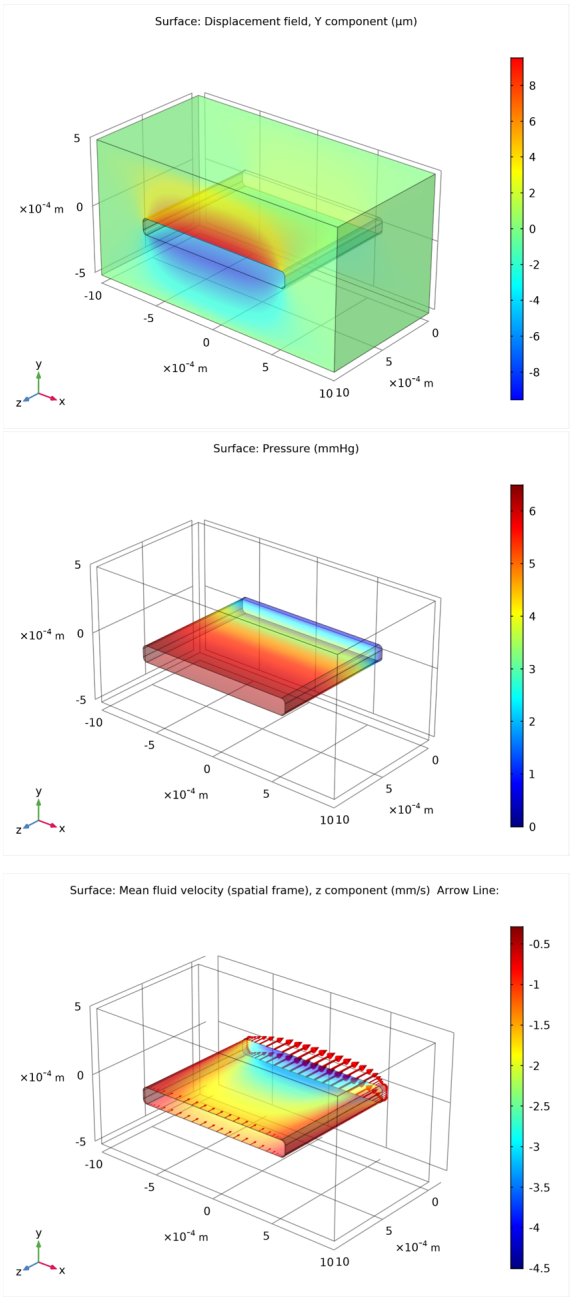

Figure 9: a) Tissue displacements results for the FDD reduced model at a $\Delta P = 6.5 mmHg$. b) AH pressure distribution for the FDD reduced model at a $\Delta P = 6.5 mmHg$. c) AH velocity distribution for the FDD reduced model at a $\Delta P = 6.5 mmHg$

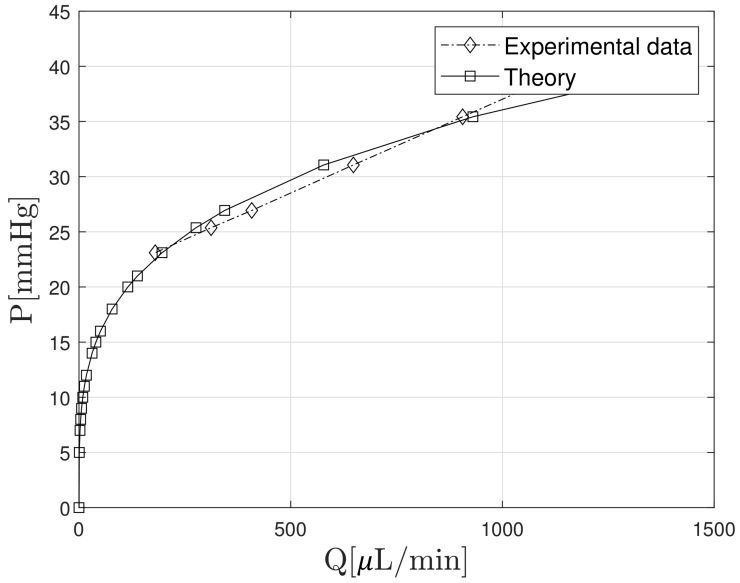

Figure 10: Pressure variation in function of the flow rate obtained from the test results and the computational simulation.

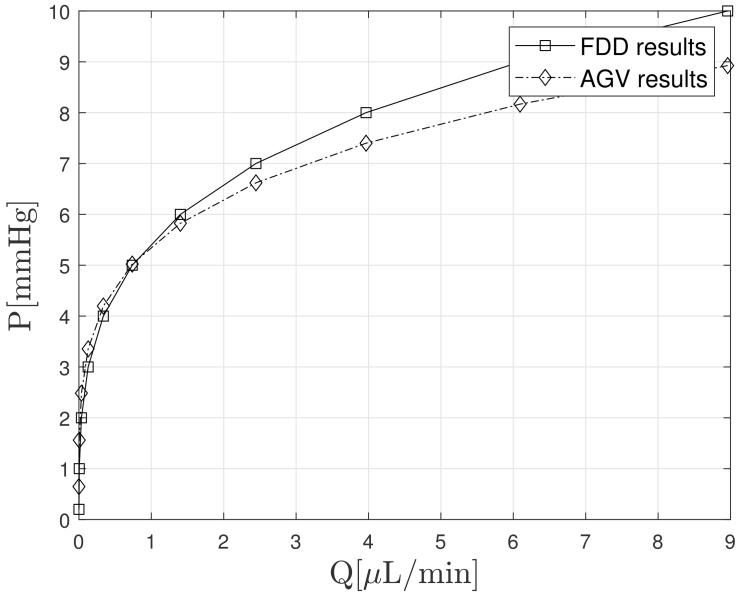

Figure 11: Pressure variation in function of the flow rate obtained from the computational simulation for a range of 0-10 mmHg.